Heliyon 10 (2024) e35507

Contents lists available at ScienceDirect

Heliyon

journal homepage: www.cell.com/heliyon

Research article

Highly reflective silver mirror enhanced by several dielectric films prepared under the low substrate temperature

Hsing-Yu Wu [a,b,c], Hong-Wei Chen [d], Shao-Rong Huang [b,e], Li-Jen Hsiao [f], Ching-Ling Cheng [e], Guo-Yu Yu [g], Yung-Shin Sun [d,*], Jin-Cherng Hsu [b,d,h,**]

[a] Taiwan Space Agency, Taiwan
[b] National Central University, Center for Astronomical Physics and Engineering, Department of Optics and Photonics, Taoyuan City, 320317, Taiwan
[c] National Yang Ming Chiao Tung University, Institute of Space Systems Engineering, Hsinchu City, 300025, Taiwan
[d] Fu Jen Catholic University, Department of Physics, New Taipei City 242062, Taiwan
[e] Diopter Precision Taiwan Co., Ltd., Taoyuan City, 324, Taiwan
[f] National United University, Department of Electrical Engineering, Miao-Li, 36063, Taiwan
[g] Department of Engineering and Technology, School of Computing and Engineering, University of Huddersfield, Queensgate, Huddersfield, HD1 3DH, UK
[h] Fu Jen Catholic University, Graduate Institute of Applied Science and Engineering, New Taipei City, 242062, Taiwan

ARTICLE INFO

Keywords:
Silver mirror
XPS
Enhanced silver coating
Silver adhesion
Space optics

ABSTRACT

Optical paths in telescopes frequently incorporate silver mirrors for high sensitivity. Unfortunately, silver mirrors without protective coatings are susceptible to sulfurization and oxidation, compromising their quality. Even with protective layers, insufficient adhesion between the coating and the silver film can lead to peeling, exposing the silver to external environments and affecting its quality. This study aimed to identify dielectric materials with superior adhesion to silver, rendering them ideal choices for silver coating applications. By electron gun evaporation, different dielectric layers were deposited on the top and bottom of the silver film under a substrate temperature below 150 °C. These coatings were composed of materials with desired refractive indices, including aluminum oxide (Al_2O_3), aluminum-doped silicon, magnesium fluoride (MgF_2), and other dielectrics. Following the deposition, a tape adhesion test was conducted to evaluate the bond strength of the samples. X-ray photoelectron spectroscopy (XPS) analysis was carried out to investigate the interaction between silver and its neighboring layers. The results revealed that Al_2O_3 and MgF_2 exhibited exceptional adhesion to silver. Moreover, these multilayer coatings can effectively enhance the reflectance of silver in the visible (VIS) wavelength ranges.

1. Introduction

Silver (Ag) exhibits outstanding optical reflectivity in the visible (VIS) and infrared (IR) spectrum, making it an ideal material for manufacturing mirrors and reflective surfaces, which are widely used in various optical devices such as reflective mirrors, polarizers, beam splitters, and reflectors for controlling light path, separating spectra, adjusting light intensity, and other purposes. In the field of

* Corresponding author.
** Corresponding author.
E-mail addresses: 089957@mail.fju.edu.tw (Y.-S. Sun), 054326@mail.fju.edu.tw (J.-C. Hsu).

https://doi.org/10.1016/j.heliyon.2024.e35507
Received 23 April 2024; Received in revised form 30 July 2024; Accepted 30 July 2024
Available online 31 July 2024

solar energy, the high reflectivity of silver mirrors can effectively focus solar light onto the collector pipes or absorbers, enhancing the efficiency of solar energy systems [1,2]. One of the most significant applications of silver mirrors lies in the construction of telescopes, deployed in space or on the ground, for observing distant objects, exploring the universe beyond our solar system, revealing details about celestial bodies, and so on. The continuous evolution of space technology has heightened the demand for telescopes that can detect various segments of the electromagnetic spectrum. Attaining high reflectance (HR) in the VIS to near-infrared (NIR) range is significant for upcoming space programs to serve commercial and research objectives [3,4].

The resolution of a telescope is limited by the size of its primary mirror, which can reach the breaking point due to limitations in grinding and polishing [5,6]. Under this circumstance, specific coatings on telescope mirrors emerge as a solution to minimize light loss as well as significantly enhance sensitivity and resolution. Metals and dielectrics are two commonly used coatings to increase the reflectance of mirrors. Dielectric coatings, also known as interference coatings, are thin films deposited on the surface of mirrors to enhance their reflective properties and control the transmission of light at specific wavelengths [7–9]. Usually, they are made from multiple layers of transparent materials with high and low refractive indices to attain interference for minimizing light loss due to reflection and maximizing the mirror's reflectivity at certain wavelengths [10]. For example, using ion-beam sputtering, Chao et al. deposited TiO_2–SiO_2 mixed film with a 17 % SiO_2 concentration to serve as high-refractive-index layers in a dielectric mirror. Experimental findings revealed that the total loss of the mirror upon deposition was 34 % less than conventional mirrors using pure TiO_2 film as high-refractive-index layers [11]. However, the refractive index of the mixed film was smaller than that of the pure TiO_2 film [12]. The mixed TiO_2 layer led to a decrease in reflectivity when compared to the pure TiO_2 layer deposited on the dielectric-metallic mirror.

Although dielectric coatings are capable of increasing the reflectance of mirrors, they are often limited by wavelength sensitivity, temperature/humidity sensitivity, mechanical durability, complex design, dependence on substrate, and cost [13–16]. As an alternative, metal- and hybrid metal-dielectric-based coatings are extensively used, especially in aerospace, defense, and military [17–20]. For example, Ag-coated mirrors were used in the telescopes for the Atmospheric Remote-sensing Infrared Exoplanet Large-survey (ARIEL) and the International Gemini Observatory [21,22]. For Cherenkov detectors, Braem et al. reported the broadband reflective coating of an aluminum (Al) film combined with one or two pairs of low- and high-index dielectric layers (MgF_2 and TiO_2, respectively) [23]. As highly efficient sunlight reflectors, metal-dielectric mirrors composed of copper (Cu)- or Al–SiO_2–TiO_2 were prepared using pulsed magnetron sputtering. It was found that these multilayer solar mirrors outperformed traditional Ag reflectors and Cu-based mirrors, which exhibited the best properties among all studied metals. In metallic coatings, Al is the most commonly used one due to its good reflectivity over a broad range of wavelengths from ultraviolet (UV) to mid-infrared (MIR) [24,25]. In addition, Al mirrors are cost-effective, durable, and mechanically stable. However, a decrease in averaged reflectivity of about 90 % was observed beyond 400 nm, accompanied by a significant decline at around 850 nm, attributed to the interband transitions of Al stack coatings [26,27]. Besides, maintaining the substrate temperature of the metallic mirror below approximately 150 °C mitigates metal oxidation during the deposition process. However, this relatively low temperature easily promotes sub-oxidation in the enhanced dielectric layers, heightening optical absorption and decreasing the reflectance of the dielectric-metal mirror.

Silver serves as an alternative for Al to attain HR in the VIS to NIR range. With a higher overall reflectivity compared to Al, particularly at around 825 nm, Ag-coated mirrors are widely used in telescopes such as the Visible and Infrared Survey Telescope for Astronomy (VISTA), the Extremely Large Telescope (ELT), and the Subaru Telescope [28,29]. The fabrication methods of Ag thin films are diverse, commonly including physical vapor deposition [30], chemical vapor deposition [31], and dc or rf magnetron sputtering [32,33]. While Ag-coated mirrors offer excellent reflectivity and optical performance, they also come with certain disadvantages, including susceptibility to tarnishing, worse durability compared to other metals, and not ideal for harsh environments [34,35]. Especially in the presence of environmental molecules such as O_2, O^-, O^{2-}, H_2O_2, SO_2, and Cl^-, the coated Ag film tends to degrade after forming compounds of Ag_2O, AgO, $AgSO_4$, AgCl, and AgS [36,37].

For this reason, additional deposited layers under and/or over the Ag film are often required to enhance its adhesion, protect it from sulfurization, and possibly increase the overall reflectivity. For example, using atomic layer deposition (ALD), AlO_x layers were deposited on top of the front surface Ag mirror to protect against oxygen plasma exposure. These AlO_x coatings having thicknesses in the vicinity of 60 nm are frequently employed for superior protection of Ag mirrors [38,39]. By ion-assisted evaporation, a durable silver coating was designed and applied to the primary mirror of the Kepler Space Telescope to optimize its reflectance from 400 nm to the NIR region. This nine-layered coating consists of Ni-CrN_x, Si_3N_4, and oxides of low and high refractive indices [40]. Wu et al. reported a multilayer, dielectric coating for the Ag mirrors of a Newtonian-type telescope. It was shown that such coating could increase the reflectivity of the mirrors in the 400–500 nm region as well as enhance their adhesion and sulfurization resistance [41].

This study aimed to investigate several dielectric layers exhibiting superior adhesion to Ag, rendering them suitable candidates for the protective coating of Ag mirrors. These dielectric layers, prepared under the relatively low substrate temperature by electron gun evaporation, included alumina (Al_2O_3), silicon dioxide (SiO_2), alumina-doped silicon dioxide (SiO_2 + 5 wt% Al_2O_3, SAO), titanium dioxide (TiO_2), magnesium fluoride (MgF_2), and niobium oxide (Nb_2O_5). Different coating configurations, incorporating various dielectrics deposited under and over the Ag film, were investigated. Following preparation, a tape adhesion test was conducted on the coated sample to evaluate its bond strength. Although these dielectric materials and their configurations are not new, detailed analyses of the interfacial bonding properties have not been performed and reported. Here, X-ray photoelectron spectroscopy (XPS) was used to explore the bonding between Ag and its protective layers. The XPS results revealed that Al_2O_3 and MgF_2 exhibited exceptional adhesion to Ag. On the one hand, Al_2O_3 or MgF_2 serves as effective protective films to prevent the silver mirror from sulfurization and preserve its quality. On the other hand, the combination layer of SiO_2 and Nb_2O_5 or MgF_2 and Nb_2O_5 is capable of enhancing the reflectivity for the detection of weak signals. These findings are of great help to designing silver mirrors in highly sensitive optical paths such as telescopes.

2. Experimental

2.1. Experimental procedure and materials

The experimental procedure is summarized in Fig. 1. As listed in Table 1, four samples were prepared on B270 substrates. A buffer layer of Al_2O_3 was deposited between the substrate and the Ag film to increase its adhesion for all samples. In sample 1, a SAO layer was coated on top of the Ag film to investigate the interfacial bonding properties. In sample 2, to increase the reflectivity in the VIS region, four alternating layers of SAO with a low refractive index and TiO_2 with a high refractive index were deposited over the Ag film. In sample 3, to test different dielectric materials, the SAO and TiO_2 layers in sample 2 were replaced with SiO_2 and Nb_2O_5 layers, respectively, with an extra Al_2O_3 layer inserted between the Ag and SiO_2 layers. The refractive index of SiO_2 closely resembles that of SAO. Nevertheless, TiO_2 has a high refractive index and may exhibit more negligible light absorption in the shorter wavelength spectrum, resulting in a slight decrease in reflectance. Finally, in sample 4, the SiO_2 layer in sample 3 was substituted with another low-refractive-index material, MgF_2. For all samples except sample 1, XPS measurements and analysis were performed before and after the tape adhesion test to investigate the sample's surface atomic composition and interfacial bonding.

2.2. Sample preparations

A B270 glass with a 25-mm diameter was used as the substrate. The substrate was first gently polished with wet cotton and CeO_2 powder, followed by a 20-min ultrasonic cleaning. Subsequently, the substrate, blown with clean nitrogen gas, was positioned on the rotating substrate holder approximately 60 cm above the deposition source. In this study, the vacuum coating system utilized was a box coater with a diameter of 90 cm (SGC-22SA-IAD, Showa Shinku Co., Yokohama, Japan). This system was equipped with a 10 kW electron beam gun and a Mark II end-Hall ion source manufactured by Veeco Ion Tech. Inc. (NY, USA). Before deposition, the vacuum chamber was evacuated to achieve a base pressure of 5×10^{-4} Pa. Following the evacuation, a 35-min ion beam cleaning process for the substrates was conducted using the grid-less end-Hall ion source with Ar as the working gas. The silver coating involved a combination of thermal evaporation of Ag and electron beam evaporation of dielectric materials. In depositing metal oxides Al_2O_3 and Nb_2O_5, the ion-assisted deposition (IAD) treatment was used, where the beam ions transferred energy to the evaporated materials, enhancing their adhesion to the substrate. For the IAD of Al_2O_3, the working gas was only Ar. For the IAD of Nb_2O_5, the gases Ar and O_2 were flowed into the chamber to ensure enough O in the metal oxide so that Nb_2O_5 instead of NbO_2 was formed. Since Ag and MgF_2 lack oxygen, they were prepared by thermal evaporation with a molybdenum boat and without IAD treatment. Table 2 lists the flow rates of the working gases (Ar and O_2) in IAD, the substrate temperatures, the deposition rates, and the thicknesses for each layer in all samples. During the deposition process, the substrate temperature was monitored and controlled by stopping deposition and natural cooling to keep it below 150 °C to prevent oxidation of the deposited metal Ag layer.

2.3. Sample characterization

XPS is a quantitative spectroscopic technique used to determine the composition of elements in materials and their chemical and electronic states. Attractive forces exist between atoms of different layers, mainly due to van der Waals forces or forces associated with atomic bonding. The latter are way stronger than the former. XPS can measure the binding energy corresponding to each intensity peak of a certain atom. If there is a lateral shift in the Gaussian curve of the peak, it suggests the possibility of bonding with atoms from another layer. In this study, depending on the sample to be measured, bond energies of Ag3d, O1s, Al2p, Ti2p, Si2p, Nb3d, Mg2p, and

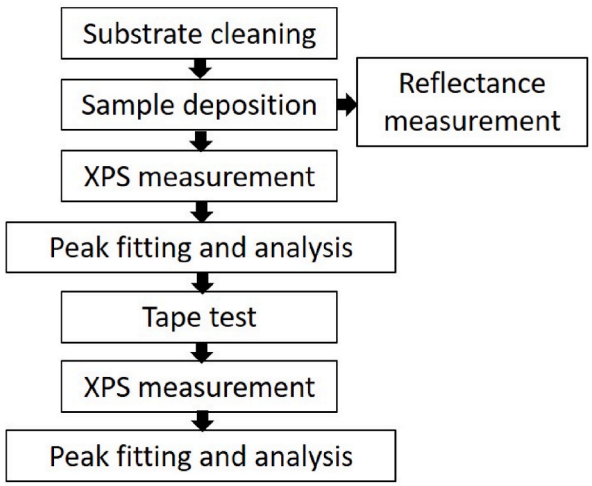

Fig. 1. Flow chart of the experimental procedure.

Table 1
Design of samples 1–4.

	sample 1 [42]	sample 2 [42]	sample 3		sample 4	
layer	material	material	material	thickness	material	thickness
1	Al_2O_3	Al_2O_3	Al_2O_3	20.4 nm	Al_2O_3	20.2 nm
2	Ag	Ag	Ag	188.2 nm	Ag	197.3 nm
3	SAO	SAO	Al_2O_3	5.2 nm	MgF_2	29.6 nm
4		TiO_2	SiO_2	37.1 nm	Nb_2O_5	48.6 nm
5		SAO	Nb_2O_5	30.4 nm	MgF_2	23.1 nm
6		TiO_2	SiO_2	80.2 nm	Nb_2O_5	30.5 nm
7			Nb_2O_5	11.8 nm		

Table 2
Deposition parameters of samples 3 and 4.

Layer	O_2 (mL/min)	Ar (mL/min)	Substrate Temp (°C)	Rate (Å/s)
Sample 3: Sub/Al_2O_3 Ag Al_2O_3 $(SiO_2\ Nb_2O_5)^2$/air				
Al_2O_3	0	9.3	120~138	1.5
Ag	–	–	124~109	15
Al_2O_3	–	–	90~96	2
SiO_2	0	9	92~112	2
Nb_2O_5	6	4.5	104~135	1
SiO_2	0	9.1	120~131	2
Nb_2O_5	6.2	4.6	118~123	1
Sample 4: Sub/Al_2O_3 Ag $(MgF_2\ Nb_2O_5)^2$/air				
Al_2O_3	0	10.4	118~136	1.5
Ag	–	–	124~108	13
MgF_2	–	–	101~87	1.5
Nb_2O_5	6	4.5	88~131	1
MgF_2	–	–	74~86	1.5
Nb_2O_5	5.9	4.6	85~126	1

F1s were identified to investigate bonding interactions between neighboring layers. For XPS depth profiling, the Versa Probe III was equipped with Ar ion-beam sputtering tools (ULVAC-PHI, Kanagawa, Japan). The Ar ion beam was operated at 5 keV and 1 μA with a typical raster size of 2 mm. A monochromatic X-ray source (Al Kα 1486.6 eV) was focused on the sample surface for XPS surface analysis. Prior to XPS scanning, the sample underwent a 1-min etching (sputtering) process to clean the film surface. In survey spectra, a pass energy of 224 eV at a 0.8-eV step was used, while in high-resolution spectra, a pass energy of 55 eV at a 0.1-eV step (for C1s, Al1s, Si2p, Mg2p, and F1s) or 69 eV at a 0.125-eV step (for Ag3d, O1s, Ti2p, and Nb3d) was applied. The C1s peak at 282.26 eV was measured and calibrated to the standard 284.8 eV. After obtaining the spectrum, the peaks were fitted to the Gaussian function using the Origin software (Ver. 8.5, OriginLab, MA, USA) to analyze the sample's atomic composition and bonding properties. For the tape adhesion test, 3M™ Scotch 600 Tape was applied to the coating surface to evaluate the adhesion of the Ag film. A spectrometer (Hitachi UH4150, Hitachi High Technologies, Tokyo, Japan) was used to measure the reflectivities of all samples in the 400–750 nm region.

3. Results

3.1. XPS analysis of samples 1 and 2

The bonding properties in the upper (SAO) and lower (Al_2O_3) interfaces of the Ag film were investigated in sample 1 in our previous study [42]. The Ag–Si and Ag–O bonds were identified as the primary bonding of Ag in the Ag/SAO and Ag/Al_2O_3 interfaces, respectively. The adhesion of Ag was attributed to these two bonds exhibiting higher binding energy than pure Ag^0. The Ag–O peak area was more dominant than the Ag–Si one, implying that the Ag film adhered better to the bottom Al_2O_3 layer than the top SAO layer. That was also verified by the tape adhesion test of sample 2 in our previous study, showing that the Ag film remained on the Al_2O_3-coated substrate, and the top $(SAO\ TiO_2)^2$ layer was partially torn off although 5-wt% Al_2O_3 dopant in SAO layer. The Ag layer was partially exposed to the air, verified by the Ag signal in the XPS survey spectrum on the surface. As a result, sample 3 was designed with 5-nm Al_2O_3 for the adhesion of the SiO_2/TiO_2 pair. Also, the high refractive index TiO_2 may exhibit slight light absorption in the short wavelength range during an unheated deposition process, reducing the reflectance.

3.2. XPS analysis of sample 3

Given that Ag adhered better to Al_2O_3 than SAO, sample 3 incorporated another Al_2O_3 layer inserted between the Ag and top enhancement layers. Also, SAO and TiO_2 layers in sample 2 were replaced with SiO_2 and Nb_2O_5 layers, respectively. Since TiO_2 shows slight light absorption in the shorter wavelength region [43], Nb_2O_5 was substituted for it in sample 3. The refractive indices of SiO_2

and Nb_2O_5 are close to those of SAO and TiO_2, respectively.

3.2.1. XPS depth profiling of sample 3

Fig. 2 shows the atomic concentrations of O1s, Nb3d, and Si2p as functions of sputtering time in the topmost Nb_2O_5–SiO_2 layers of sample 3. In the Nb_2O_5 layer (time = 1–2 min), the concentrations of Nb and O are approximately 35 % and 65 %, respectively, indicating the formation of Nb_2O_5 and possibly some NbO_2. After 4 min, SiO_2 is detected by showing concentrations of around 30 % and 70 % for Si and O, respectively.

Fig. 3 shows the XPS depth profiling and Nb_2O_5–SiO_2 interfacial fine scan of O1s, Nb3d, and Si2p of sample 3. In Fig. 3(a), the O signal increases gradually with the etching depth, indicating the transition from the outmost Nb_2O_5 to the subsequent SiO_2 layers. The content of O is higher in the SiO_2 than in the Nb_2O_5 layers. Fig. 3(b) indicates the fine scan XPS of O1s in the Nb_2O_5/SiO_2 interface at about 3-min sputtering. After curve fittings, three peaks are identified at around 531.0, 531.5, and 533.0 eV, which can be attributed to O in NbO_2, Nb_2O_5, and SiO_2, respectively [44]. The formation of NbO_2 is possibly due to the sub-oxidation of Nb_2O_5 as a result of insufficient oxygen supply during the coating process.

The Nb3d depth profiling in Fig. 3(c) indicates Nb's decrease and vanishing as the etching goes deeper from Nb_2O_5 to SiO_2. In the etching time of 1 min, the clear two-peak stoichiometric Nb_2O_5 at the surface results from the oxidation in the air. In Fig. 3(d), the fine scan of Nb3d in the interface at about a 3-min sputtering time suggests the existence of both Nb3d3/2 and Nb3d5/2 peaks [45]. For the Nb3d5/2 peak, two sub-peaks at around 205.0 and 206.5 eV are identified, corresponding to Nb in NbO_2 and Nb_2O_5 respectively [46]. The Nb3d3/2 peak is also decomposed into two sub-peaks, as determined in Fig. 3(d) [45]. For Nb in Nb_2O_5, a spin-orbit splitting of about 3.5 eV is assigned to the core levels of Nb^{5+}.

The Si2p depth profiling in Fig. 3(e) shows an increasing Si signal as the etching depth increases. In Fig. 3(f), the corresponding fine scan at the interface indicated a clear Si peak located at approximately 103.3 eV and attributed to Si in SiO_2 [44].

3.2.2. Surface XPS after tape adhesion test of sample 3

After undergoing the tape adhesion test, XPS analysis was performed on the surface of sample 3 to investigate the remaining components. Fig. 4(a) shows the XPS survey spectrum of the surface. The atomic concentrations of O1s, C1s, Nb3d, Si2p, and Al2p are about 48.3, 40.8, 16.8, 2.1, and 2.0 %, respectively. The carbon signal is present due to the tape residue remaining after peeling off the surface. The existing signal is the protection layers of Nb_2O_5 on the top enhancement layer. Some tiny dust particles might originate from our clean lab or deposition vacuum systems. These particles could stick to the substrate before deposition. This loosely attached dust was dislodged and created tiny holes during XPS measurements, revealing the SiO_2 and Al_2O_3 layers. As a result, XPS signals were emitted from the SiO_2 and Al_2O_3 layers in the pinhole. The concentration of the Ag signal is less than 0.1 %, which implies that the Ag film is exposed to the air only in the pinholes due to the strong Ag–O bonding between Ag and its bottom/top Al_2O_3. That is qualitatively seen in Fig. 4(b), which displays the peeled tape after the adhesion test. Visually, no deposited layer adhered to the tape, suggesting that both the enhancement layers Al_2O_3 (SiO_2 Nb_2O_5)^2 and the Ag film adhered very well to the substrate.

The fine scan XPS of O1s in Fig. 5(a) indicates the existence of two sub-peaks. The one located at around 530.1 eV is close to the reported 530.3 eV of SiO_2–C–O–Nb bonding [47]. The carbon binding comes from the residual tape after the adhesion test. The Si–O–C binding comes from the glass substrate or the SiO_2 layer in the deposited film's pinhole defects, which are exposed to the incident X-ray during the XPS measurement [48]. The other sub-peak at approximately 531.2 eV is attributed to Nb_2O_5. The 207.2-eV and 209.9-eV peaks in Fig. 5(b) correspond to Nb3d5/2 and Nb3d3/2 in Nb_2O_5, respectively. That shows the Nb_2O_5 stoichiometry at the sample's surface, as described in Section 3.2.1.

In the fine scan of Si2p XPS shown in Fig. 5(c), two sub-peaks at 101.7 and 103.4 eV are identified. The 101.7-eV one is from the Si–O–C bonding, as reported by Kura et al. [48], while the 103.4-eV one comes from the Si in SiO_2 [44].

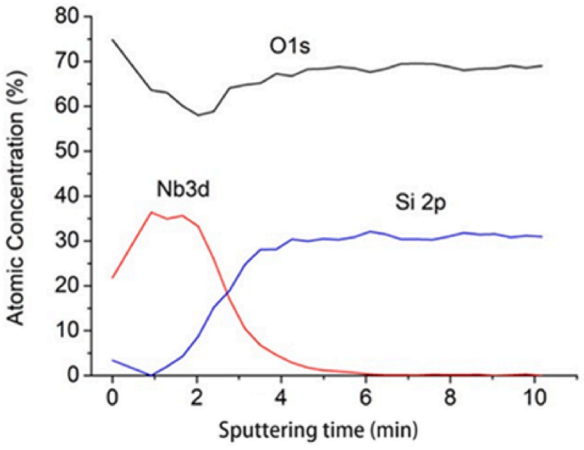

Fig. 2. Atomic concentrations at different sputtering times in XPS depth profiling of the topmost Nb_2O_5–SiO_2 layers in sample 3.

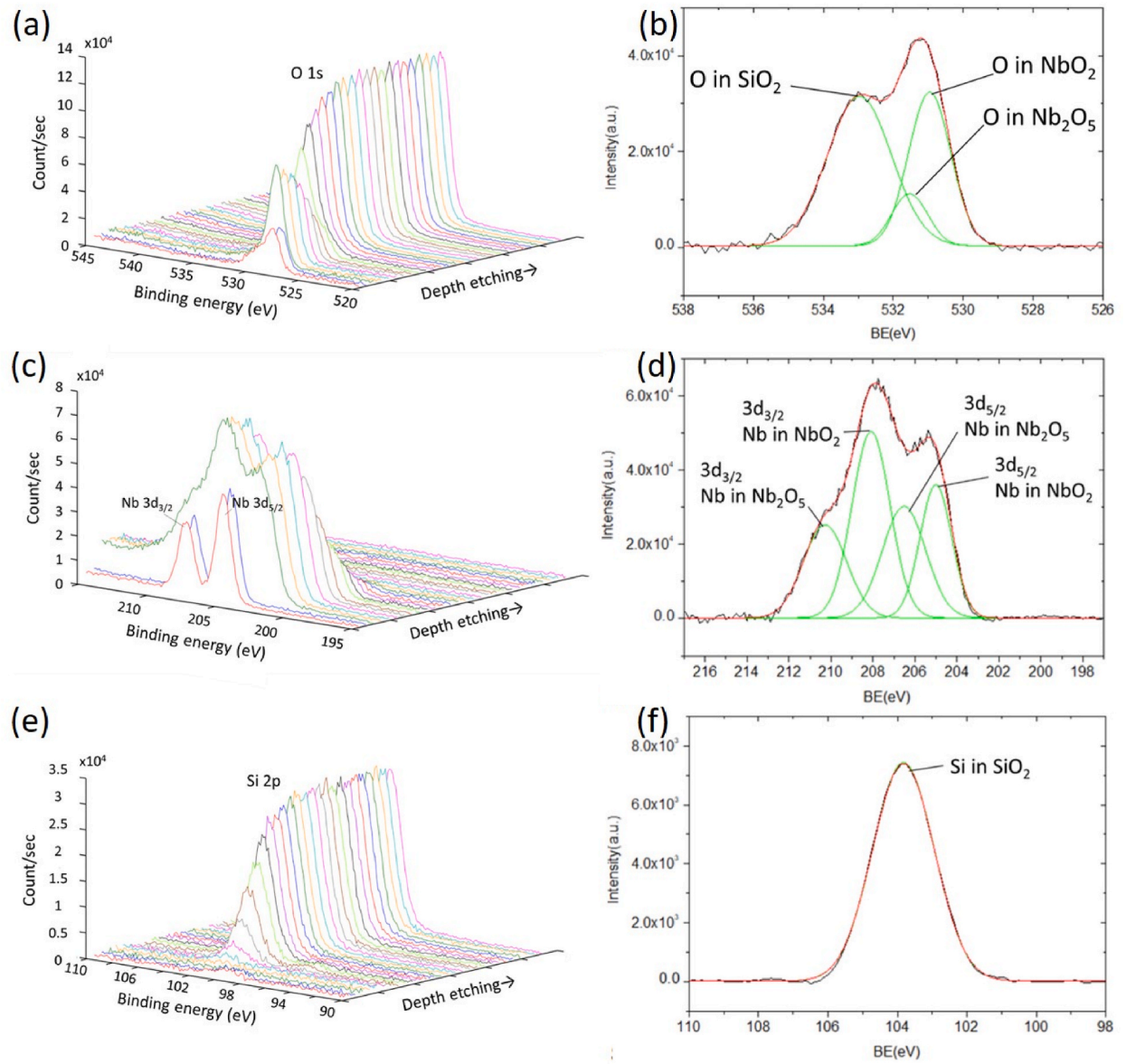

Fig. 3. XPS depth profiling of (a) O1s, (c) Nb3d, and (e) Si2p of sample 3; fine scan XPS of (b) O1s, (d) Nb3d, and (f) Si2p in the Nb_2O_5/SiO_2 interface of sample 3.

Fig. 5(d) displays the Nb3p XPS and small Ag3d XPS. The Ag3d XPS exhibits two main peaks of Ag3d5/2 and Ag3d3/2 located at 368.4 and 374.5 eV, respectively. These values are close to the standard Ag^0 peaks, suggesting that the Ag atoms in this sample are in a non-ionic/metallic state [49]. Each of these two peaks can be further decomposed into two fitted curves. In the Ag3d5/2 peak, the one with lower binding energy at around 367.9 eV but a higher intensity is attributed to the Ag^0 bonding [44]. The other has a slightly higher binding energy at about 368.8 eV, but a lower intensity corresponds to the Ag–O bonding between the Ag and Al_2O_3 layers [50]. The formation of the Ag–O bonding at the interface arises from the charge transfer of metallic silver, where electrons migrate from the valence band to a higher energy conduction band in an excited state of silver atoms [42]. This bonding is suggested to exist in a covalent state without charge polarization [51].

3.3. XPS analysis of sample 4

The SiO_2 layer in sample 3 was replaced with another low-refractive-index material MgF_2, which could increase the reflectivity of the dielectric-metallic mirror. As an inorganic compound, MgF_2 is transparent in the UV to IR region and has a relatively low thermal expansion coefficient, making it suitable for multilayer optical coatings of high reflection [52,53].

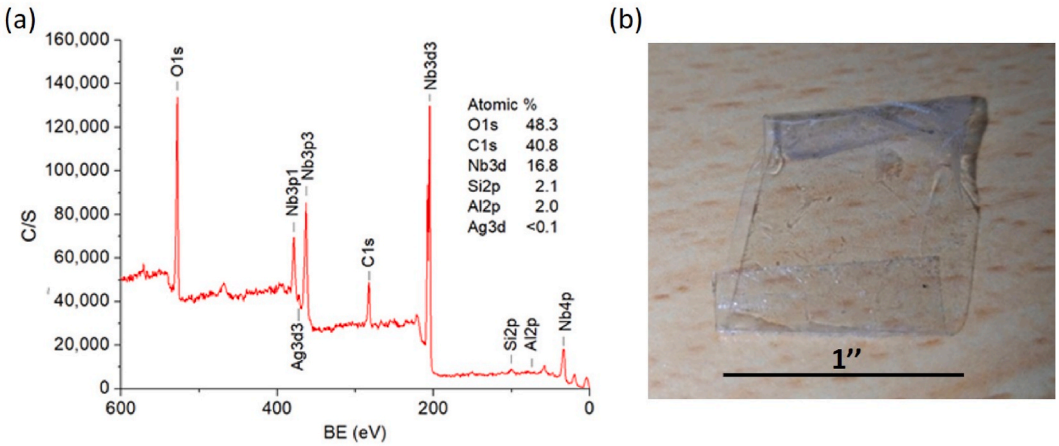

Fig. 4. (a) XPS survey spectrum of sample 3 after the tape adhesion test. (b) Peeled tape after the adhesion test on sample 3.

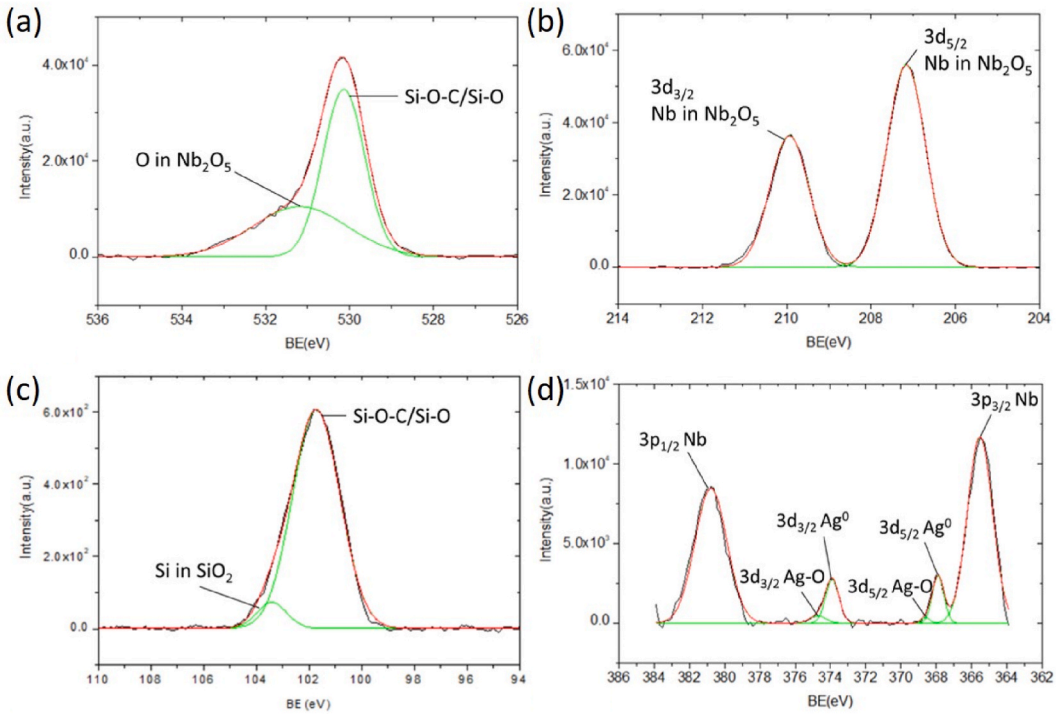

Fig. 5. XPS fine scan of (a) O1s, (b) Nb3d, (c) Si2p, and (d) Ag3d on the surface of sample 3 after the tape adhesion test.

3.3.1. XPS depth profiling of sample 4

Fig. 6 indicates the atomic concentrations of O1s, Nb3d, F1s, Mg2p, and Ag3p as functions of sputtering time in the enhancement layer of sample 4. The signals of all elements, except Ag, change periodically, suggesting the existence of successive Nb_2O_5, MgF_2, Nb_2O_5, and MgF_2 layers. In the MgF_2 layer, the concentrations of F and Mg are about 60 and 32 %, respectively, suggesting its approximated stoichiometry. In the Nb_2O_5 layer, the atomic concentration ratio of O to Nb is lower than 2.5 except for the ratio at the sample's surface, possibly due to the presence of NbO_2.

The XPS depth profiling and Nb_2O_5–MgF_2 interfacial fine scan of O1s, Nb3d, Mg2p, and F1s of sample 4 are displayed in Fig. 7. The depth profile of O1s, as illustrated in Fig. 7(a), shows the highest intensity at the outermost layer of Nb_2O_5, which gradually decreases at the next MgF_2 layer. The intensity increases again at the second Nb_2O_5 layer and decreases again at the second MgF_2 layer, similar to the atomic concentration of O1s shown in Fig. 6. The fine scan of O1s in the Nb_2O_5–MgF_2 interface, presented in Fig. 7(b), is similar to Fig. 3(b) except for the absence of the 533.0-eV peak originating from SiO_2. Decomposition of the main peak reveals the presence of O from NbO_2 at 531.0 eV and Nb_2O_5 at 531.5 eV [44].

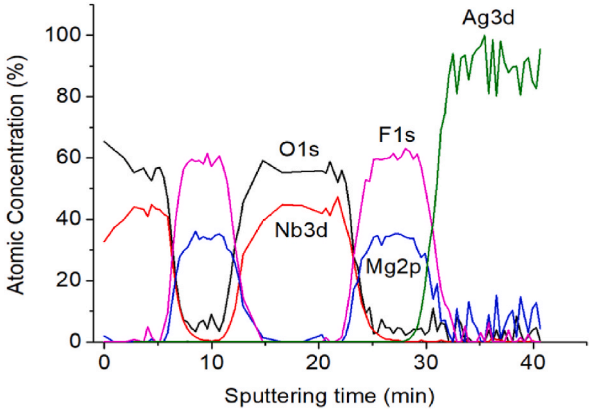

Fig. 6. Atomic concentrations at different sputtering times in XPS depth profiling of sample 4.

The depth profiling of Nb3d in Fig. 7(c) again shows the periodic presence and absence of Nb as a result of the alternating Nb_2O_5 and MgF_2 layers. The clear two-peak stoichiometric Nb_2O_5 at the surface results from the oxidation in the air. A combined peak appears when the etching depth is increased. After decomposing the combined Nb3d5/2 peak at the etching time of about 6 min in Fig. 7(d), two sub-peaks located at 203.3 and 205.5 eV are attributed to Nb in NbO_2 and Nb_2O_5, respectively [46]. The intensity ratio between Nb in Nb_2O_5 and Nb in NbO_2 in Fig. 7(d) is more significant than that in Fig. 3(d) because of the lower oxygen chemical absorption for the MgF_2 layer.

The depth profiling of Mg2p in Fig. 7(e) indicates that the signal of Mg increases gradually as the etching goes from Nb_2O_5 to MgF_2. The corresponding interfacial fine scan in Fig. 7(f) exhibits a clear peak at 52. 5 eV from Mg in MgF_2 [44]. As presented in Fig. 7(g), the signal of F1s in its XPS depth profiling changes periodically, being almost zero, gradually increasing to a maximum, decreasing to zero again, and slowly arriving at the peak once more. A main peak is observed in the interfacial fine scan of F1s shown in Fig. 7(h). After decomposition, a dominant sub-peak at around 686.9 eV is identified and attributed to F in MgF_2 [54]. The higher binding energy results from the Ag center of the large electronegativity strongly attracting electrons from the weakly polarizable, hard fluoride anion [55]. The other weak peak, located at approximately 684.90 eV, possibly originates from the formation of a tiny amount of NbF_5 at the Nb_2O_5/MgF_2 interface [56].

To investigate the adhesion of Ag to its upper MgF_2, the XPS depth profiling of Ag3d and the interfacial fine scan in the MgF_2–Ag interface were performed and displayed in Fig. 8. As indicated in Fig. 8(a), the signal of Ag gradually appears as the etching goes from the enhancement layer to the Ag film. Maximum intensities of around 5.5×10^5 and 6.5×10^5 count/sec were attained within the Ag layer for the Ag3d3/2 and Ag3d5/2 peaks, respectively. In the MgF_2–Ag interface, two peaks of Ag3d3/2 and Ag3d5/2 are identified, as shown in Fig. 8(b), each being decomposed into two sub-peaks. As Fig. 5(d) shows in the Ag3d5/2 peak, the sub-peak has a lower binding energy of about 367.98 eV, but a higher intensity originates from the Ag^0 bonding [44]. The other exhibits a slightly higher binding energy of approximately 368.56 eV, but a lower intensity can be attributed to the non-ionic Ag–F bonding between Ag and MgF_2. Such bonding is not ionic because the binding energy of Ag in AgF is lower than that of Ag^0 in metal Ag [57].

3.3.2. Surface XPS after tape adhesion test of sample 4

The tape adhesion test was conducted on sample 4, followed by the surface XPS analysis. As indicated in the survey spectrum of Fig. 9(a), the atomic concentrations of C1s, O1s, Nb3d, Mg2p, and Al2p are about 39.5, 35.0, 15.5, 4.4, and 3.9 %, respectively. Again, the signal of carbon probably comes from surface tape residues. Although F1s is hardly detected, signals from other elements suggest the presence of residual enhancement/protection layers Nb_2O_5 and MgF_2. The atomic concentration of Ag is less than 0.1 %, implying that the Ag layer was not exposed to the air. This, in turn, verifies the strong adhesion of Ag to its upper MgF_2 and lower Al_2O_3 layers via Ag–F and Ag–O bonding, respectively. After the adhesion test, the peeled tape is shown in Fig. 9(b). Again, no obvious residues are visually observed, suggesting that the enhancement layers $(MgF_2/Nb_2O_5)^2$ and the Ag film adhere very well to the B270 glass slide.

The fine scan XPS of O1s in Fig. 10(a) is similar to that observed in Fig. 5(a) of sample 3. The sub-peaked at around 530.1 eV can be attributed to the SiO_2–C–O–Nb bonding. The carbon binding comes from the residual tape. The SiO_2 binding comes from the glass substrate in the film's pinhole defects, which are exposed to the incident X-ray during the XPS measurement [58]. The other sub-peak at approximately 531.6 eV originates from O in Nb_2O_5, also shown in the fine scan of Nb3d in Fig. 10(b). The existence of both Nb3d5/2 and Nb3d3/2 in Nb_2O_5 is observed at about 207.3 and 209.9 eV, respectively. That illustrates the Nb_2O_5 stoichiometry at the sample's surface, as shown in the skin-depth profiling in Figs. 6 and 7(c).

The fine scan of Mg2p is illustrated in Fig. 10(c). Ignoring the signal of the Mg 2p plasmon at around 60 eV, two sub-peaks were identified at 49.2 and 50.9 eV after peak fittings. The one with higher binding energy comes from the Mg in MgF_2, as Zhang et al. reported in the multilayer coating of MgF_2 XPS [59]. The other one with lower binding energy is attributed to the Mg in $Mg(OH)_2$ due to the exposure of Mg to moisture in the air [44]. In the fine Ag3d scan of Fig. 10(d), four main peaks of Nb3p1/2, Ag3d3/2, Ag3d5/2, and Nb3p3/2 from high to low binding energies are similar to those observed in Fig. 5(d). The two Ag peaks are further decomposed into two sub-peaks resulting from the non-ionic/metallic states [49]. In the Ag3d5/2 peak, the one having lower binding energy at

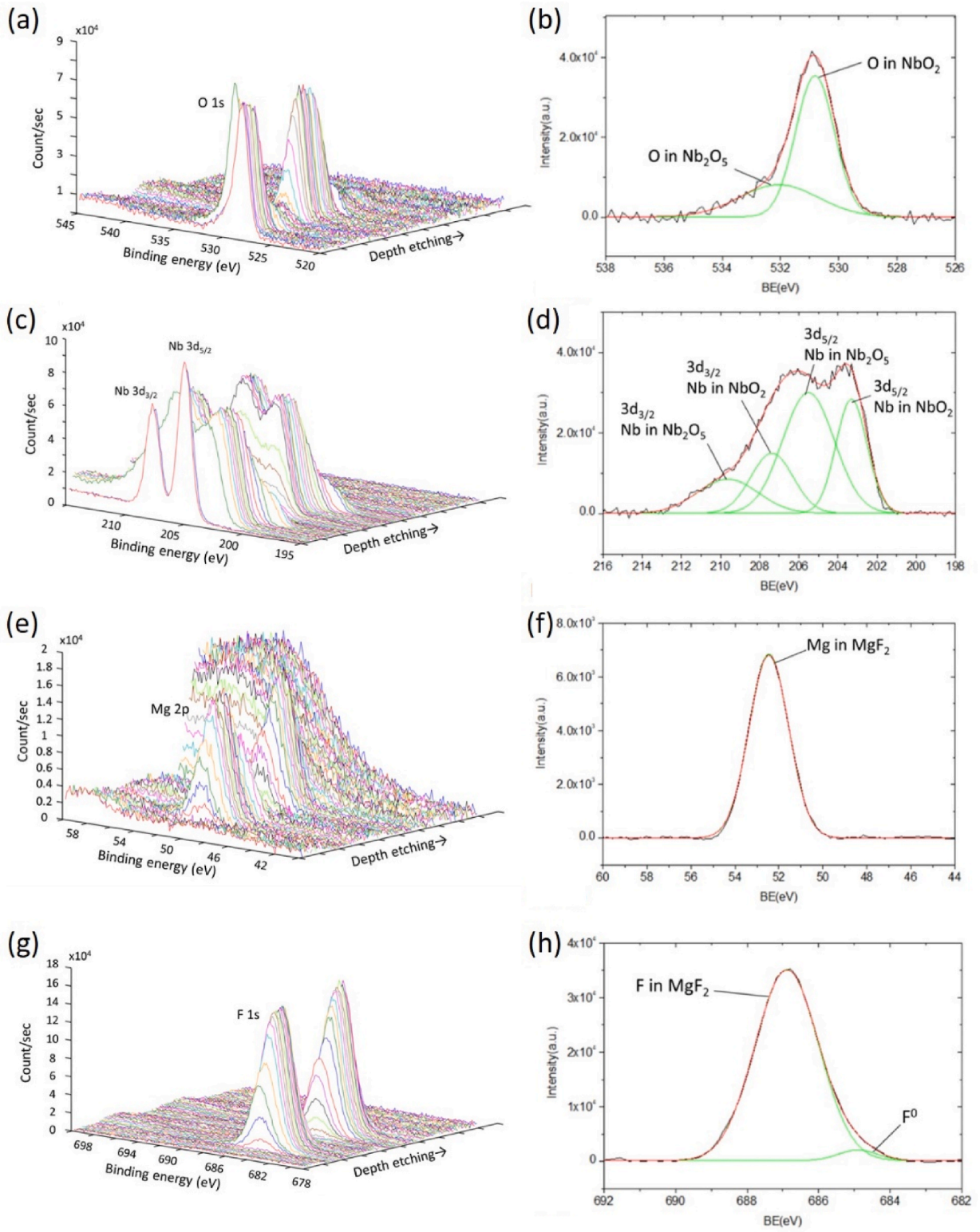

Fig. 7. XPS depth profiling of (a) O1s, (c) Nb3d, (e) Mg2p, and (g) F1s of sample 4; fine scan XPS of (b) O1s, (d) Nb3d, (f) Mg2p, and (h) F1s at the Nb_2O_5/MgF_2 interface of sample 4.

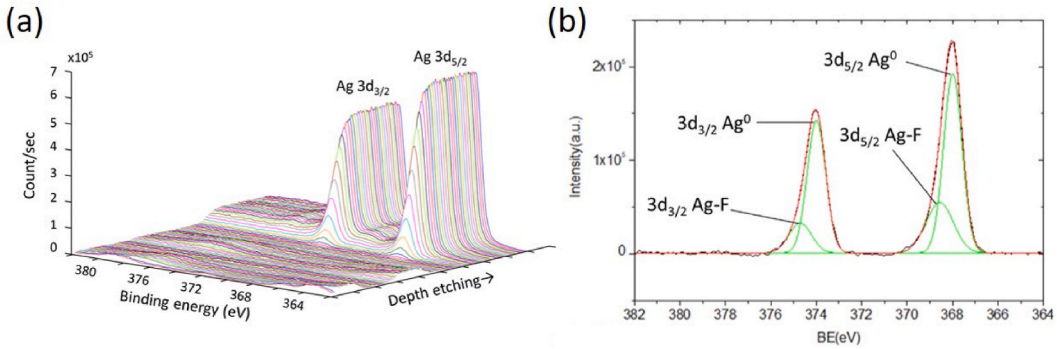

Fig. 8. (a) XPS depth profiling and (b) fine scan of Ag3d in the Ag/MgF_2 interface of sample 4 before the tape adhesion test.

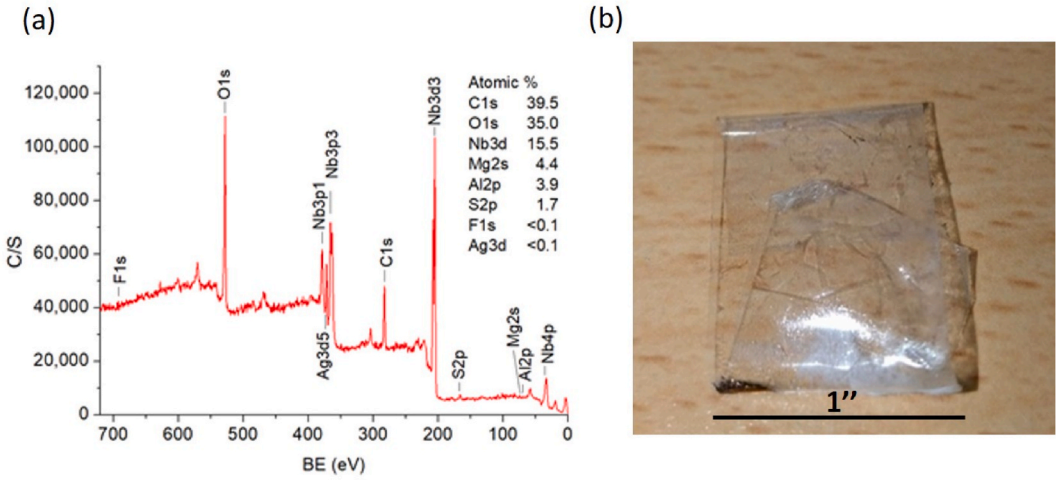

Fig. 9. (a) XPS survey spectrum of sample 4 after the tape adhesion test. (b) Peeled tape after the adhesion test on sample 4.

about 368.1 eV but a much higher intensity is attributed to the Ag^0 bonding [44]. The other, with slightly higher binding energy at around 368.65 eV but much lower intensity, comes from the Ag–F bonding between the Ag and MgF_2 layers [50]. The increasing binding energy of the Ag–F bonding to increase the adhesion of the enhancement coatings is similar to that of the Ag–O bonding in our previous study [42].

3.4. Comparison of reflectivities of samples 2–4

The reflectivities of samples 2–4 and pure silver in the VIS region are shown in Fig. 11. For pure Ag film without enhanced dielectric coatings, the reflectivity is higher than 97 % in the wavelength range above 460 nm, but it drops to 94 % below 460 nm. Samples 2–4, with multilayer coatings on the Ag film, can achieve reflectivities of over 96 % in the VIS range. Sample 2 maintains a reflectivity above 97 % except for a 430–475 nm dip. Sample 3 exhibits a reflectivity above 97 % in the VIS range except for a slight decrease to 96.9 % in the 455–490 nm range. Sample 4 shows the highest overall reflectance among all samples. It attains a reflectivity above 98 % except for a slight decrease to 97.9 % in the 550–590 nm range. These results suggest that these multilayer films can effectively enhance the reflectance of the Ag layer in the shorter wavelength range (430–475 nm) with the average reflectivities in that region being 96.8 %, 96.4 %, 97.0 %, and 99.0 % for pure silver, Samples 2, 3, and 4, respectively.

4. Discussion

Enhancement coatings are additional layers of materials applied to the surface of a silver mirror to enhance its specific properties, such as reflectance, durability, and protection against environmental factors. Dielectric materials like Al_2O_3, SiO_2, and MgF_2 can be deposited onto the silver mirror as protective layers. The interfacial bonding between Ag and the dielectric layer was investigated by XPS. As reported in our previous study and indicated in Fig. 5(d) and 8(b) [42], Ag–O, Ag–Si, and Ag–F bonds at the Ag/Al_2O_3, Ag/SAO, and Ag/MgF_2 interfaces were identified as the primary bonding of Ag layer, respectively. The F1s binding energy in Fig. 7 (h) is also higher than the common value. They illustrated the higher binding energies at the Ag interfacial surfaces due to the Ag center

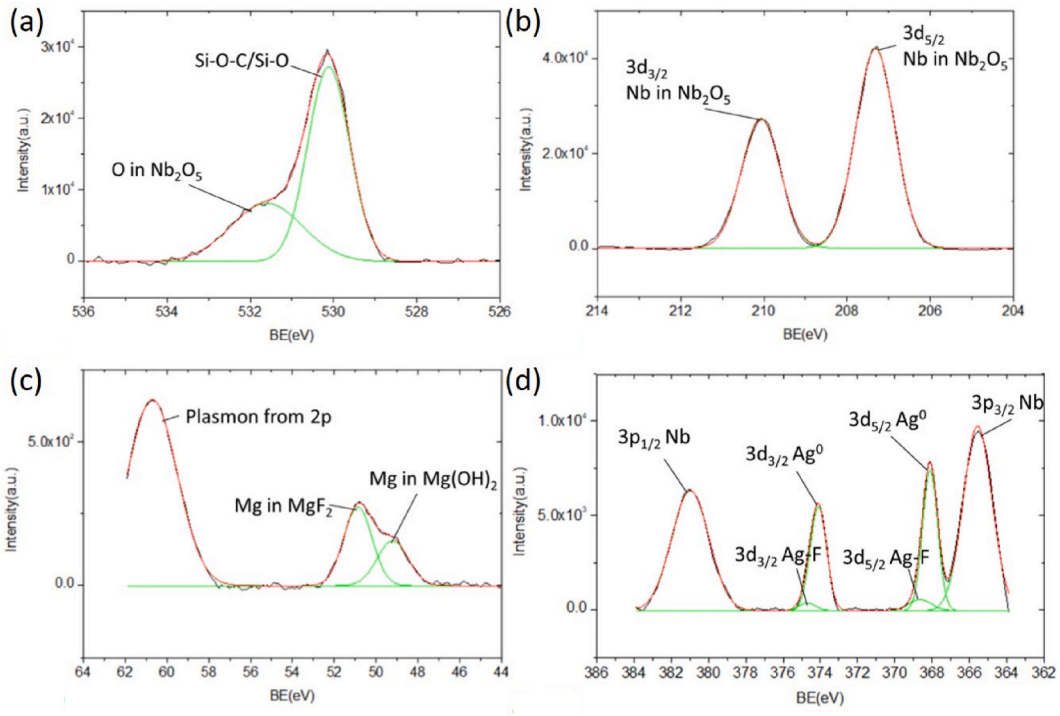

Fig. 10. XPS fine scan of (a) O1s, (b) Nb3d, (c) Mg2p, and (d) Ag3d on the surface of sample 4 after the tape adhesion test.

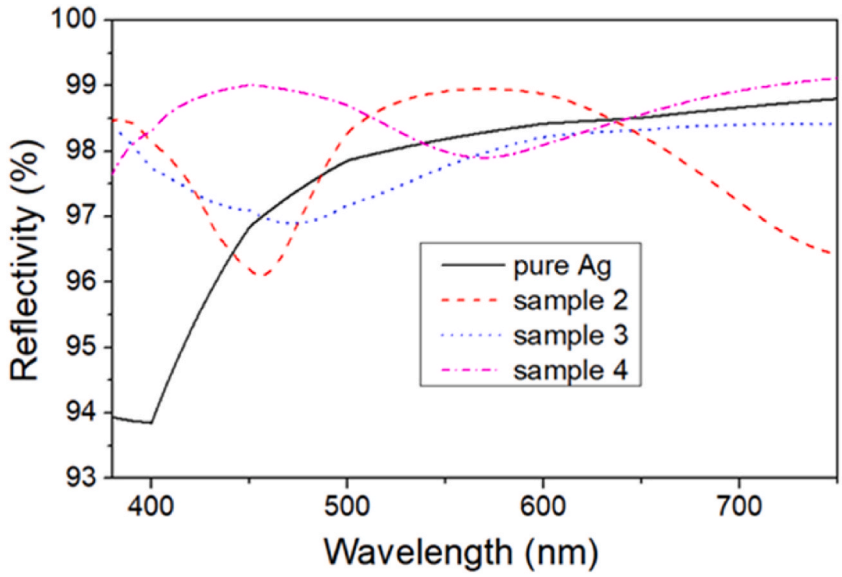

Fig. 11. Reflectivities of samples 2–4 and pure silver mirror.

strongly attracting electrons from the weakly polarizable anions [55]. Moreover, the bonding between Ag and Al_2O_3 was stronger than between Ag and SiO_2. Xu et al. explored the interfacial adhesion of pure silver films to three low-refractive index coatings (MgF_2, Al_2O_3, and SiO_2) using typical peel and moisture testing methods [60]. They found that the adhesion between Al_2O_3 and Ag layers was significantly higher than between MgF_2 and Ag, while the adhesion between MgF_2 and Ag layers was significantly higher than between SiO_2 and Ag layers. For pure Al_2O_3 fabricated by ALD, a thickness exceeding 15 nm was reported to exhibit the optimal protection without impacting the absolute reflectivity of a silver mirror within the spectral range of 320–2500 nm [61]. In the present multilayer coating, the thickness of the protective Al_2O_3 layer was only around 5 nm.

A dielectric multilayer configuration can be used with combinations of alternating high and low refractive indices to improve the

reflectance properties of silver mirrors. In this study, the reflectance properties of a multilayer comprising of $(SAO/TiO_2)^2$, $(SiO_2/Nb_2O_5)^2$, or $(MgF_2/Nb_2O_5)^2$ were tested. SAO, SiO_2, and MgF_2 have low refractive indices, while TiO_2 and Nb_2O_5 have high refractive indices. Fig. 11 suggests that all these designs enhanced the reflectance of silver, especially in the wavelength range below 460 nm. As reported by Sidqi et al., combining high-index pure oxide materials with silicon dioxide has been shown to reduce absorption and scatter losses in combinations such as TiO_2–SiO_2, Nb_2O_5–SiO_2, and ZrO_2–SiO_2 films [11,62].

In our previous study, the chemical states of the sub-oxide titanium (Ti^{3+} and Ti^{2+}) were still produced in the TiO_2 film, although the film was deposited in oxygen ambient by ion beam sputtering deposition (IBSD) and post-annealed at 450 °C for 6 h [43]. The result of the sub-oxide titanium unfavored the enhanced layer in the short wavelength region. Therefore, the Nb_2O_5 layer of the almost high-refraction material was investigated to replace the enhanced TiO_2 layer in the study.

Moreover, MgF_2 is a significant fluoride, characterized by its consistently low refractive index and low extinction coefficient across a broad spectral range from the far-ultraviolet (FUV) to the mid-infrared (MIR). Additionally, it exhibits minimal absorption, satisfactory mechanical durability, low coefficient of thermal expansion, and transparency in the UV to IR region. MgF_2, having a lower index of ~1.38 than SiO_2 of ~1.46 at 550-nm wavelength, favors increasing the reflectivity and its wavelength region from VIS to IR due to the more significant difference between the high and low indices of the films [63]. Finally, sample 4 with the enhancement layer of $(MgF_2/Nb_2O_5)^2$ deposited on the silver layer exhibited the highest overall reflectivity of around 98 % in the entire VIS region and passed the tape adhesion test. The MgF_2/Nb_2O_5 bilayer films with different periods (two, four, and six periods) were used to fabricate the green-light (500 nm) distributed Bragg reflectors (DBRs), showing higher reflective ratios compared with calculated values [64].

5. Conclusions

Different dielectric material combinations were designed and deposited onto the silver layer to explore their impact on enhancing the silver's protection and reflectance properties. All samples involve a configuration of dielectrics of alternating high and low refractive indices. In these samples, Ag–O, Ag–Si, and Ag–F bonds were identified as the primary bonding of Ag in the Ag/Al_2O_3, Ag/SAO, and Ag/MgF_2 interfaces, respectively. The tape adhesion test and the following XPS analysis of sample 2 indicated that the Ag–O bonding was stronger than the Ag–Si one [42]. Therefore, Al_2O_3 and MgF_2 were considered good candidates for the protection layer to enhance the adhesion of Ag.

In terms of reflectance enhancement, combinations of $(SiO_2/Nb_2O_5)^2$ and $(MgF_2/Nb_2O_5)^2$ performed better (with higher reflectivities) than that of $(SAO/TiO_2)^2$ in the range of 430–475 nm, with all excelling un-coated Ag film, especially in the wavelength range below 460 nm. The results of this study can be applied to reflective mirrors in high-sensitivity optical systems. On the one hand, Al_2O_3 or MgF_2 can be utilized as effective protective layers to prevent the silver mirror from coming into contact with the external environment, thus safeguarding it from sulfurization that may compromise its quality. On the other hand, the combination of SiO_2 and Nb_2O_5 layers, or the combination of MgF_2 and Nb_2O_5 layers, is suitable for enhancing the reflectivity of the mirror. This, in turn, enables efficient reflection of weak signals in the VIS to NIR region for the space mirror.

Data availability statement

The data that support the findings of this study are available from the corresponding author upon reasonable request.

CRediT authorship contribution statement

Hsing-Yu Wu: Funding acquisition, Conceptualization. **Hong-Wei Chen:** Validation, Formal analysis, Data curation. **Shao-Rong Huang:** Validation, Methodology, Formal analysis, Data curation. **Li-Jen Hsiao:** Resources, Conceptualization. **Ching-Ling Cheng:** Resources, Conceptualization. **Guo-Yu Yu:** Resources, Conceptualization. **Yung-Shin Sun:** Writing – review & editing, Writing – original draft, Resources. **Jin-Cherng Hsu:** Writing – review & editing, Writing – original draft, Project administration, Methodology, Funding acquisition, Conceptualization.

Declaration of competing interest

The authors declare that they have no known competing financial interests or personal relationships that could have appeared to influence the work reported in this paper.

Acknowledgments

This study is supported by the National Science and Technology Council of Taiwan under project Nos. 112-2112-M-030-002, 111-2221-E-030-007, and Control Optics Taiwan Inc.

References

[1] C.M. López, J.D.P. Bueno, J.A.C. Mendez, R.H. Leos, M.L.M. López, A.S. Domínguez, Y.M. Vong, Deterioration of novel silver coated mirrors on polycarbonate used for concentrated solar power, Sustainability-Basel 14 (2022).

[2] H. Jamali, Investigation and review of mirrors reflectance in parabolic trough solar collectors (PTSCs), Energy Rep. 5 (2019) 145–158, https://doi.org/10.1016/j.egyr.2019.01.006.
[3] S.D. Dibb, J.F. Bell, L.T. Elkins-Tanton, D.A. Williams, Visible to near-infrared reflectance spectroscopy of asteroid (16) psyche: implications for the psyche mission's science investigations, Earth Space Sci. 10 (2023).
[4] J. de León, J. Licandro, C.D. Marcos, R.D. Marcos, L.M. Lara, F. Moreno, N. Pinilla-Alonso, M. Serra-Ricart, M. De Prá, G.P. Tozzi, et al., Visible and near-infrared observations of interstellar comet 2I/Borisov with the 10.4-m GTC and the 3.6-m TNG telescopes, Mon Not R Astron Soc 495 (2020) 2053–2062, https://doi.org/10.1093/mnras/staa1190.
[5] M. Metwally, F. Eltohamy, T.M. Bazan, Design of very high-resolution satellite telescopes Part III: telescope size reduction, Ieee T Aero Elec Sys 57 (2021) 4044–4050, https://doi.org/10.1109/Taes.2021.3088424.
[6] M. Metwally, T.M. Bazan, F. Eltohamy, Design of very high-resolution satellite telescopes Part I: optical system design, Ieee T Aero Elec Sys 56 (2020) 1202–1208, https://doi.org/10.1109/Taes.2019.2929969.
[7] M.A. Kats, R. Blanchard, P. Genevet, F. Capasso, Nanometre optical coatings based on strong interference effects in highly absorbing media, Nat. Mater. 12 (2013) 20–24, https://doi.org/10.1038/Nmat3443.
[8] G. Winkler, L.W. Perner, G.W. Truong, G. Zhao, D. Bachmann, A.S. Mayer, J. Fellinger, D. Follman, P. Heu, C. Deutsch, et al., Mid-infrared interference coatings with excess optical loss below 10 ppm, Optica 8 (2021) 686–696, https://doi.org/10.1364/Optica.405938.
[9] M.A. Kats, F. Capasso, Ultra-thin optical interference coatings on rough and flexible substrates, Appl. Phys. Lett. 105 (2014).
[10] C.C. Lee, J.C. Hsu, D.H. Wong, The characteristics of some metallic oxides prepared in high vacuum by ion beam sputtering, Appl. Surf. Sci. 171 (2001) 151–156, https://doi.org/10.1016/S0169-4332(00)00556-0.
[11] S. Chao, W.H. Wang, C.C. Lee, Low-loss dielectric mirror with ion-beam-sputtered TiO-SiO mixed films, Appl Optics 40 (2001) 2177–2182, https://doi.org/10.1364/Ao.40.002177.
[12] J.C. Hsu, C.C. Lee, Single- and dual-ion-beam sputter deposition of titanium oxide films, Appl. Opt. 37 (1998) 1171–1176, https://doi.org/10.1364/ao.37.001171.
[13] M. Niittymäki, K. Lahti, T. Suhonen, J. Metsäjoki, Effect of temperature and humidity on dielectric properties of thermally sprayed alumina coatings, Ieee T Dielect El In 25 (2018) 908–918, https://doi.org/10.1109/Tdei.2018.006892.
[14] J. Shen, S.H. Liu, Z.C. Shen, J.D. Shao, Z.X. Fan, Theoretical analysis of optical properties of dielectric coatings dependence on substrate subsurface defects, Appl. Surf. Sci. 252 (2006) 3855–3860, https://doi.org/10.1016/j.apsusc.2005.06.005.
[15] G.T. West, P.J. Kelly, Improved durability of dielectric coatings for large-area applications on glass via ion beam pretreatment of the substrate, J. Vac. Sci. Technol. A 24 (2006) 334–339, https://doi.org/10.1116/1.2172947.
[16] S.E. Watkins, J.P. Black, B.J. Pond, Optical scatter characteristics of high-reflectance dielectric coatings and fused-silica substrates, Appl. Opt. 32 (1993) 5511–5518, https://doi.org/10.1364/AO.32.005511.
[17] D. Garoli, L.V.R. De Marcos, J.I. Larruquert, A.J. Corso, R.P. Zaccaria, M.G. Pelizzo, Mirrors for space telescopes: degradation issues, Appl Sci-Basel 10 (2020).
[18] M. Holynska, A. Tighe, C. Semprimoschnig, Coatings and thin films for spacecraft thermo-optical and related functional applications, Adv Mater Interfaces 5 (2018).
[19] S. Joseph, D. Yadlovker, O. Marcovitch, H. Zipin, Evaluating environmental survivability of optical coatings, in: Proceedings of the SPIE Defense, Security, and Sensing, Orlando, Florida, United States, 2009, p. 73020I.
[20] R. Moore, H. Torres, R. DeLuca, M. Gentile, K.C. Zadrovicz, M. Albrecht, S. Kohli, Salt spray resistant silver coatings for aerospace and defense applications, in: Proceedings of the SPIE Defense + Commercial Sensing, United States, Orlando, Florida, 2023, p. 125300C.
[21] P. Chioetto, P. Zuppella, V. Da Deppo, E. Pace, G. Morgante, L. Terenzi, D. Brienza, N. Missaglia, G. Bianucci, S. Spinelli, et al., Qualification of the thermal stabilization, polishing and coating procedures for the aluminum telescope mirrors of the ARIEL mission, Exp. Astron. 53 (2022) 885–904, https://doi.org/10.1007/s10686-022-09852-x.
[22] M. Boccas, T. Vucina, C. Araya, E. Vera, C. Ahhee, Protected-silver coatings for the 8-m Gemini telescope mirrors, Thin Solid Films 502 (2006) 275–280, https://doi.org/10.1016/j.tsf.2005.07.295.
[23] A. Braem, C. David, C. Joram, Metal multi-dielectric mirror coatings for Cherenkov detectors, Nucl Instrum Meth A 553 (2005) 182–186, https://doi.org/10.1016/j.nima.2005.08.074.
[24] J. Hennessy, K. Balasubramanian, C.S. Moore, A.D. Jewell, S. Nikzad, K. France, M. Quijada, Performance and prospects of far ultraviolet aluminum mirrors protected by atomic layer deposition, J Astron Telesc Inst 2 (2016), https://doi.org/10.1117/1.Jatis.2.4.041206.
[25] G. Hass, J.B. Heaney, W.R. Hunter, Reflectance and preparation of front surface mirrors for use at various angles of incidence from the ultraviolet to the far infrared, Phys. Thin Films 12 (1982) 1–51.
[26] A.C. Phillips, J. Miller, W. Brown, D. Hilyard, B. Dupraw, V. Wallace, D. Cowley, Progress toward high-performance reflective and anti-reflection coatings for astronomical optics, in: Proceedings of the SPIE Astronomical Telescopes + Instrumentation, Marseille, France, 2008, p. 70185A.
[27] A.C. Phillips, W.E. Brown, B. Dupraw, D.F. Hilyard, D.J. Cowley, Progress toward high-performance astronomical coatings, in: Proceedings of the SPIE Astronomical Telescopes + Instrumentation, San Diego, California, United States, 2010, p. 77393Y.
[28] S. Schwinde, S. Shestaeva, R. Holzlöhner, G. Willers, R. Schlegel, A. Förster, R. Parra, S. Guisard, O. Sqalli, S. Schröder, Development of advanced silver coatings for telescope mirrors, in: Proceedings of the SPIE Astronomical Telescopes + Instrumentation Montréal, Québec, Canada, 2022, p. 121881X.
[29] T. Kurakami, M. Yutani, T. Kanzawa, N. Ohshima, S.S. Hayashi, T. Usuda, S. Kubota, Mirror coating 2003 in Subaru telescope, in: Proceedings of the SPIE Astronomical Telescopes + Instrumentation, Glasgow, United Kingdom, 2004.
[30] M. Nur-E-Alam, M.K. Basher, M. Vasiliev, N. Das, Physical vapor-deposited silver (Ag)-Based metal-dielectric nanocomposites for thin-film and coating applications, Appl Sci-Basel 11 (2021).
[31] L.A. Brook, P. Evans, H.A. Foster, M.E. Pemble, A. Steele, D.W. Sheel, H.M. Yates, Highly bioactive silver and silver/titania composite films grown by chemical vapour deposition, J Photoch Photobio A 187 (2007) 53–63, https://doi.org/10.1016/j.jphotochem.2006.09.014.
[32] A. Rizzo, M.A. Tagliente, M. Alvisi, S. Scaglione, Structural and optical properties of silver thin films deposited by RF magnetron sputtering, Thin Solid Films 396 (2001) 29–35, https://doi.org/10.1016/S0040-6090(01)01242-1.
[33] J. Mashaiekhy, Z. Shafieizadeh, H. Nahidi, Effect of substrate temperature and film thickness on the characteristics of silver thin films deposited by DC magnetron sputtering, Eur. Phys. J. Appl. Phys. 60 (2012).
[34] C. Atkinson, C.L. Sansom, H.J. Almond, C.P. Shaw, Coatings for concentrating solar systems - a review, Renew Sust Energ Rev 45 (2015) 113–122, https://doi.org/10.1016/j.rser.2015.01.015.
[35] A. García-Segura, A. Fernández-García, M.J. Ariza, F. Sutter, L. Valenzuela, Durability studies of solar reflectors: a review, Renew Sust Energ Rev 62 (2016) 453–467, https://doi.org/10.1016/j.rser.2016.04.060.
[36] T.E. Graedel, Corrosion mechanisms for silver exposed to the atmosphere, J. Electrochem. Soc. 139 (1992).
[37] D.K. Burge, E. BennettH, E.J. Ashley, Effect of atmospheric exposure on the infrared reflectance of silvered mirrors with and without protective coatings, Appl Optics 12 (1973) 42–47.
[38] D.M. Fryauf, A.C. Phillips, N.P. Kobayashi, Critical processing temperature for high-performance protected silver mirrors, J Astron Telesc Inst 7 (2021).
[39] D.M. Fryauf, J.J.D. Leon, A.C. Phillips, N.P. Kobayashi, Effect of intermediate layers on atomic layer deposition-aluminum oxide protected silver mirrors, J Astron Telesc Inst 3 (2017).
[40] D.A. Sheikh, S.J. Connell, R.S. Dummer, Durable silver coating for Kepler Space Telescope primary mirror, in: Proceedings of the SPIE Astronomical Telescopes + Instrumentation, Marseille, France, 2005, p. 70104E.
[41] H.Y. Wu, S.R. Huang, C.H. Shih, L.J. Hsiao, H.W. Chen, M.C. Cheng, J.C. Hsu, Highly reflective silver-enhanced coating with high adhesion and sulfurization resistance for telescopes, Nanomaterials-Basel 12 (2022).

[42] H.Y. Wu, H.W. Chen, S.R. Huang, C.H. Shih, G.Y. Yu, Y.S. Sun, J.C. Hsu, Characterization of silver layers deposited by aluminum oxide, silicon dioxide, and blend for highly reflective optics, Opt. Mater. 149 (2024).
[43] J.C. Hsu, C.C. Lee, H.L. Chen, C.C. Kuo, P.W. Wang, Investigation of thin TiO films cosputtered with Si species, Appl. Surf. Sci. 255 (2009) 4852–4858, https://doi.org/10.1016/j.apsusc.2008.12.016.
[44] J.F. Moulder, W.F. Stickle, P.E. Sobol, K.D. Bomben, Handbook of X-Ray Photoelectron Spectroscopy, Physical Electronics , Inc., United States of America, 1995, 6509 Flying Cloud Drive Eden Prairie , Minnesota 55344.
[45] V.I. Chukwuike, K. Rajalakshmi, R.C. Barik, Surface and electrochemical corrosion analysis of niobium oxide film formed in various wet media, Applied Surface Science Advances 4 (2021).
[46] A. Gupta, M. Mittal, M.K. Singh, S.L. Suib, O.P. Pandey, Low temperature synthesis of NbC/C nano-composites as visible light photoactive catalyst, Sci Rep-Uk 8 (2018).
[47] B. Sivaranjini, R. Mangaiyarkarasi, V. Ganesh, S. Umadevi, Vertical alignment of liquid crystals over a functionalized flexible substrate, Sci Rep-Uk 8 (2018).
[48] A. Kaur, P. Chahal, T. Hogan, Selective fabrication of SiC/Si diodes by excimer laser under ambient conditions, Ieee Electr Device L 37 (2016) 142–145, https://doi.org/10.1109/Led.2015.2508479.
[49] C.H. Zhao, J.L. Du, D.W. Huang, Y.Q. Li, J.H. Chen, W.Z. Li, Microstructure and strong optical absorption property of the Ag/AlO nano-films, J Alloy Compd 671 (2016) 419–423, https://doi.org/10.1016/j.jallcom.2015.11.226.
[50] Y.W. Lu, X.W. Du, J. Sun, X. Han, S.A. Kulinich, Influence of surface Si-Ag bonds on photoluminescence of porous silicon, J. Appl. Phys. 100 (2006).
[51] A. Al-Sarraj, K.M. Saoud, A. Elmel, S. Mansour, Y. Haik, Optoelectronic properties of highly porous silver oxide thin film, SN Appl. Sci. 3 (2021) 1–13.
[52] F. Perales, J.M. Herrero, D. Jaque, C.D.L. Heras, Improvement of MgF thin coating films for laser applications, Opt. Mater. 29 (2007) 783–787, https://doi.org/10.1016/j.optmat.2006.01.001.
[53] A. Arroussi, M. Ghezali, First-principles study of the structural, electronic and optical properties of MgF, Optik 164 (2018) 16–27, https://doi.org/10.1016/j.ijleo.2018.03.010.
[54] S.H. Woo, C.K. Hwangbo, Effects of annealing on the optical, structural, and chemical properties of TiO and MgF thin films prepared by plasma ion-assisted deposition, Appl Optics 45 (2006) 1447–1455, https://doi.org/10.1364/Ao.45.001447.
[55] W. Grochala, R.G. Egdell, P.P. Edwards, Z. Mazej, B. Zemva, On the covalency of silver-fluorine bonds in compounds of Silver(I), Silver(II) and Silver(III), ChemPhysChem 4 (2003) 997–1001, https://doi.org/10.1002/cphc.200300777.
[56] S.H. Yuan, F. Qian, S.M. Yang, Y. Cai, Q. Wang, J. Sun, Z.K. Liu, S.Z.NbF. Liu, A novel α-phase stabilizer for FA-based perovskite solar cells with high efficiency, Adv. Funct. Mater. 29 (2019), https://doi.org/10.1002/adfm.201807850.
[57] J. Lee, S.H. Choi, G. Im, K.J. Lee, T. Lee, J. Oh, N. Lee, H. Kim, Y. Kim, S. Lee, et al., Room-temperature anode-less all-solid-state batteries via the conversion reaction of metal fluorides, Adv Mater 34 (2022).
[58] X.X. Song, Q. Wang, H.F. Liu, G.B. Dou, H.J. Li, W.J. Wu, F. Hui, J.Q. Fan, J. Liu, L.C. Tu, A method for alleviating the effect of pinhole defects in inter-metal dielectric films, J. Micromech. Microeng. 29 (2019).
[59] W.N. Zhang, K. Hu, J.L. Tu, A. Aierken, D.L. Xu, G.Y. Song, X.Y. Sun, L. Li, K.T. Chen, D.Y. Zhang, et al., Broadband graded refractive index TiO/AlO/MgF multilayer antireflection coating for high efficiency multi-junction solar cell, Sol. Energy 217 (2021) 271–279, https://doi.org/10.1016/j.solener.2021.01.012.
[60] X.K. Xu, Z.S. Tang, J.D. Shao, Z.X. Fan, The study on the interface adhesion comparison of the MgF, AlO, SiO and Ag thin films, Appl. Surf. Sci. 245 (2005) 11–15, https://doi.org/10.1016/j.apsusc.2004.10.018.
[61] P. Bulkin, S. Gaiaschi, P. Chapon, D. Daineka, N. Kundikova, Protective coatings for front surface silver mirrors by atomic layer deposition, Opt Express 28 (2020) 15753–15760, https://doi.org/10.1364/Oe.388546.
[62] N. Sidqi, C. Clark, G.S. Buller, G.K.V.V. Thalluri, J. Mitrofanov, Y. Noblet, Comparative study of dielectric coating materials for micro-cavity applications, Opt. Mater. Express 9 (2019) 3452–3468, https://doi.org/10.1364/Ome.9.003452.
[63] H.A. Macleod, Thin-film Optical Filters, fourth ed., CRC Press/Taylor & Francis, Boca Raton, FL, 2010, p. 782, xviii.
[64] D. Yong, B.S. Chen, J.J. Lin, H.W. Tseng, Y.L. Wu, C.F. Yang, Fabrication of 500 nm distributed Bragg reflector using NbO-MgF multi-layer films, Mod. Phys. Lett. B 35 (2021).